DOI: 10.1002/adsc.200800374

Selective Hydrogen Oxidation Catalysts *via* Genetic Algorithms

Jurriaan Beckers,[a,*] Frédèric Clerc,[b] Jan Hendrik Blank,[a] and Gadi Rothenberg[a,*]

[a] Van 't Hoff Institute for Molecular Sciences, University of Amsterdam, Nieuwe Achtergracht 166, 1018 WV Amsterdam, The Netherlands
Fax: (+31)-20-525-5604; e-mail: J.Beckers@uva.nl or G.Rothenberg@uva.nl
[b] IRCELYON – CNRS, 2, Avenue Albert Einstein, 9626 Villeurbanne, France

Received: June 13, 2008; Revised: August 1, 2008; Published online: September 26, 2008

Abstract: Solid "oxygen reservoirs," such as doped ceria, can be successfully applied in a novel process for the oxidative dehydrogenation of propane. The ceria lattice oxygen selectively burns hydrogen from the dehydrogenation mixture at 550 °C. This gives three key advantages: it shifts the dehydrogenation equilibrium to the desired product side, generates heat *in situ,* which aids the endothermic dehydrogenation, and simplifies product separation. We have applied a genetic algorithm to screen doped cerias for their performance in the selective hydrogen oxidation. Three generations of doped ceria catalysts (61 catalysts in total), were synthesised. Dopants were chosen from a set of 26 elements, and with a maximum of two dopants per catalyst, at five different concentrations. The catalyst performance (activity and selectivity), is expressed by a fitness value. Each generation shows a higher average fitness value. The dopant type has a large effect on the catalyst fitness. We identified six dopant atoms which lead to selective hydrogen combustion catalysts, namely bismuth (Bi), chromium (Cr), copper (Cu), potassium (K), manganese (Mn), lead (Pb) and tin (Sn) ("good" dopants). Analysis of the effect of electronegativity, ionic radius and dopant concentration shows that most elements yielding a high fitness have electronegativities ranging from 1.5–1.9. Generally, the properties of catalysts containing two dopants can be predicted from the behaviour of singly doped ones. Synergy does occur for certain copper-, iron- and platinum-containing catalysts. The addition of calcium (Ca) or magnesium (Mg) to copper-doped catalysts doubles the activity, and the selectivity of iron doped catalysts can be improved by adding chromium (Cr), manganese (Mn) or zirconium (Zr). Importantly, the doped cerias show a high stability in the redox cycling, much higher than that of supported oxides. A Cr- and Zr-doped catalyst ($Ce_{0.90}Cr_{0.05}Zr_{0.05}O_2$) was highly selective and active over 250 redox cycles (a total of 148 h on stream), with no phase segregation or change in particle size.

Keywords: cerium dioxide (ceria, CeO_2); data mining; doped ceria; evolutionary algorithm; oxidative dehydrogenation; X-ray diffraction (XRD)

Introduction

Selective oxidation is applied in the production of many important bulk chemicals and intermediates, such as acrolein, acrylic acid, MTBE, and maleic anhydride.[1] In these processes, the value of the hydrocarbons is increased by selective addition of oxygen atoms, and the greatest challenge is preventing overoxidation. Selective oxidation can also, however, remove certain species by combusting them. This is the case in oxidative dehydrogenation, which can be used to obtain propene from propane (Scheme 1).[2–9] Propane dehydrogenation is an endothermic reaction, but oxidative dehydrogenation can overcome this limitation. Selectively combusting the formed hydrogen into water generates heat *in situ* and shifts the equilibrium towards the product side.

We recently introduced a new type of oxidative dehydrogenation system, employing doped cerias as solid oxygen reservoirs (SORs).[10,11] The dehydrogenation step is performed over a conventional Pt-Sn-Al_2O_3 catalyst, and the hydrogen is combusted using the oxygen of the ceria lattice (Scheme 1, *left*).[12] After the ceria has been reduced, the lattice oxygen vacancies are re-filled using air, creating a cyclic redox process (Scheme 1, *right*) and simultaneously burning off any coke. This is safer than mixing gaseous O_2 and H_2 at high temperatures (typically 500–600 °C). Furthermore, the use of two catalysts allows for separate tuning of the hydrogen combustion and the dehydrogenation. Supported metal oxides can also perform this selective hydrogenation, but they sinter under redox cycling.[13–17] Ceria has high temperature stability and a facile $Ce^{3+} \rightleftarrows Ce^{4+} + e^-$ reac-

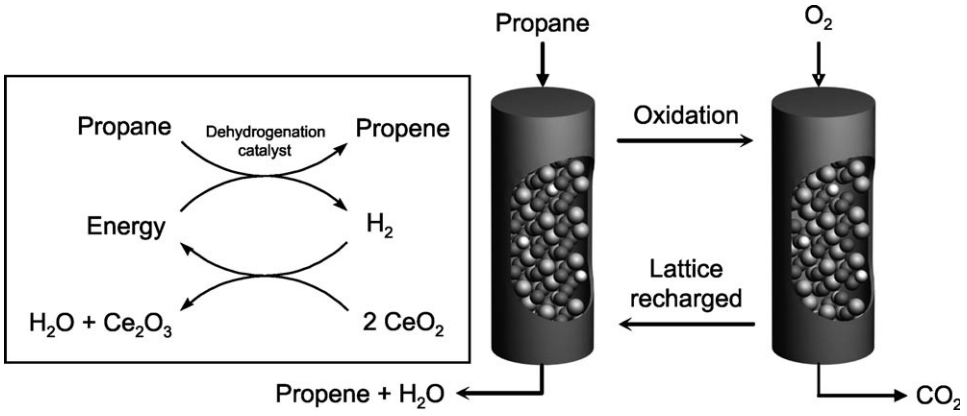

Scheme 1. *Left:* the reactions occurring during the combined propane dehydrogenation and selective hydrogen combustion. The dehydrogenation consumes energy and yields hydrogen. The hydrogen combustion consumes hydrogen and yields energy. *Right:* Cartoon showing a proposed reactor configuration for the redox process, enabling continuous production of high purity propene. Whilst the propane dehydrogenation and selective hydrogen combustion are performed in the left-hand reactor, the catalysts in the right-hand reactor are being regenerated (coke combustion and refilling of the lattice oxygen for the solid oxygen reservoir).

tion, making it a good SOR.[18] CeO_2 itself, however, is not selective, but we showed that selectivity, activity and stability can be tuned by doping the ceria lattice with different cations.[10] In a preliminary screening, we tested ten catalysts for their selectivity towards hydrogen combustion from a mix with ethane and ethene, with the dopant type as the only variable. A tungsten-doped catalyst showed excellent selectivity and stability for this reaction.[10] In this study, we screen doped ceria catalysts for hydrogen combustion from a mix with propane and propene. Twenty-six different dopants are used, at five possible concentrations, with a maximum of two dopants per catalyst. This yields a huge amount of catalyst candidates. Synthesising and testing all of the combinations is not practical. Instead, we employ a genetic algorithm (GA), to find the optimal catalyst using an iterative approach. GAs mimic evolutionary biology *in silico*.[19–21] Compared with the almost ubiquitous application of GAs in other scientific fields, few researchers have used an evolutionary approach for screening heterogeneous catalysts. Baerns et al. have studied the oxidative dehydrogenation of propane, using gaseous oxygen,[22–24] total propane oxidation,[25] and the production of hydrocyanic acid.[26] Yamada et al. have investigated methanol synthesis,[27–29] and others have performed studies on (selective) oxidation,[30–33] reduction,[34] methane reforming,[35] and isomerisation.[36] Most of the catalysts used in these studies are mixed oxides containing four to five different metals. Kim et al. have used doped cerias for the reforming of methane.[35]

In this paper, we present the results of a genetic algorithm-based catalyst optimisation. A total of 61 doped cerias are evaluated for their performance in selective hydrogen combustion. The evolution of the fitness value over three generations is evaluated, and the performance of the catalysts is correlated to their composition.

Results and Discussion

Catalyst Preparation and Characterisation

Catalysts were prepared by co-melting a mixture of the metal nitrate hydrate precursors (chlorides or ammonium metallates were used when nitrates were not available).[11,37] After the precursor has liquefied, the pressure was lowered and a solid mixed-metal nitrate formed. This was converted into the mixed oxide by calcining in static air at 700 °C for 5 h. The following notation is used: **Gn–m**, where **n** is the generation number and **m** is the catalyst number. The activity, selectivity and fitness value of all 61 catalysts are given in Table 1, together with the catalyst composition and characterisation data. The fitness function is defined as: $F = [\text{selectivity} + (0.2 \times \text{activity})/120] \times 100$, and ranges from 0–100. Note that specific attributes of some of the catalysts are presented in detail thereafter.

Figure 1 shows pictures of three catalysts after heating at reduced pressure (*top*, mixed nitrates), and after calcination (*bottom*, mixed oxides). Whereas pure cerium nitrate is white, and CeO_2 is pale yellow, the mixed oxides show a variety of colours. These ceria-based mixed oxides have the general catalyst formula $Ce_{1-x-y}M^1_xM^2_yO_2$. The metals M^1 and M^2 are added at zero, two, five, eight or ten mol%, and chosen from 26 candidates (*vide infra*). Each catalyst

Table 1. Composition, characterisation data and catalytic performance of doped cerias **1-61**.

Catalyst	Composition[a]	Surface area [$m^2 g^{-1}$]	Crystallite size [nm][b]	Lattice parameter [Å][c]	Activity [% H_2 converted]	H_2 oxidation selectivity [%]	Fitness value[d]
G1–01	$Ce_{0.87}Al_{0.08}Ta_{0.05}O_2$	58	nd	nd	0	0	0
G1–02	$Ce_{0.96}Ca_{0.02}Sr_{0.02}O_2$	42	nd	nd	0.4	18	21
G1–03	$Ce_{0.89}Cr_{0.02}Fe_{0.09}O_2$	28	nd	nd	9	85	82
G1–04	$Ce_{0.96}Pd_{0.04}O_2$	53	nd	nd	0	0	0
G1–05	$Ce_{0.98}Sn_{0.02}O_2$	67	12	5.408	8	77	75
G1–06	$Ce_{0.89}Pt_{0.02}Mn_{0.09}O_2$	57	nd	nd	0	0	0
G1–07	$Ce_{0.90}Ta_{0.05}Ti_{0.05}O_2$	46	nd	nd	0	0	0
G1–08	$Ce_{0.92}Zr_{0.02}Mg_{0.08}O_2$	26	nd	nd	0	0	0
G1–09	$Ce_{0.90}Nd_{0.10}O_2$	61	14	5.430	0	0	0
G1–10	$Ce_{0.90}Yb_{0.08}Gd_{0.02}O_2$	24	nd	nd	1	40	39
G1–11	$Ce_{0.90}Ru_{0.05}Sm_{0.05}O_2$	65	nd	nd	0	0	0
G1–12	$Ce_{0.90}Y_{0.05}Sr_{0.05}O_2$	27	nd	nd	0.4	44	42
G1–13	$Ce_{0.90}Bi_{0.05}K_{0.05}O_2$	17	nd	nd	18[e]	91	87
G1–14	$Ce_{0.91}La_{0.09}O_2$	49	nd	nd	0	0	0
G1–15	$Ce_{0.90}W_{0.10}O_2$	25	26	5.411	0	0	0
G1–16	$Ce_{0.92}Cr_{0.08}O_2$	24	26	5.414	15	86	83
G1–17	$Ce_{0.90}Fe_{0.10}O_2$	50	14	5.404	0	0	0
G1–18	$Ce_{0.90}Cu_{0.10}O_2$	47	15	5.411	7	89	85
G1–19	$Ce_{0.90}Bi_{0.10}O_2$	33	18	5.416	33[e]	77	81
G1–20	$Ce_{0.91}Mn_{0.09}O_2$	56	11	5.407	5	93	83
G1–21	$Ce_{0.91}Ca_{0.09}O_2$	22	28	5.416	0	0	0
G1–22	$Ce_{0.92}Pb_{0.08}O_2$	56	13	5.411	46[e]	92	93
G1–23	$Ce_{0.90}Pd_{0.10}O_2$	72	13	5.411	0	0	0
G1–24	CeO_2	36[1]	25[1]	5.409[1]	0	0	0
G1–25	$Ce_{0.90}Zr_{0.10}O_2$	71	nd	nd	1	36	36
G2–01	$Ce_{0.90}Yb_{0.10}O_2$	nd	18	5.406	0	0	0
G2–02	$Ce_{0.86}Ca_{0.09}Cu_{0.05}O_2$	nd	24	5.411	18	87	84
G2–03	$Ce_{0.90}Cr_{0.05}Bi_{0.05}O_2$	31	28	5.412	38 [e]	84	87
G2–04	$Ce_{0.87}Mg_{0.05}Cu_{0.08}O_2$	nd	18	5.409	17	87	84
G2–05	$Ce_{0.90}Mn_{0.02}Fe_{0.08}O_2$	nd	16	5.405	4	87	78
G2–06	$Ce_{0.84}Zr_{0.08}Cu_{0.08}O_2$	54	17	5.411	13	92	88
G2–07	$Ce_{0.87}Bi_{0.08}Sn_{0.05}O_2$	55	14	5.411	45 [e]	84	87
G2–08	$Ce_{0.96}Gd_{0.02}Bi_{0.02}O_2$	nd	19	5.412	7	68	68
G2–09	$Ce_{0.88}Cr_{0.02}W_{0.10}O_2$	nd	21	5.409	1	36	36
G2–10	$Ce_{0.90}Zr_{0.02}Fe_{0.08}O_2$	nd	14	5.402	2	78	71
G2–11	$Ce_{0.90}Al_{0.10}O_2$	nd	13	5.408	0	0	0
G2–12	$Ce_{0.90}Al_{0.02}Cu_{0.05}O_2$	52	14	5.409	11	89	85
G2–13	$Ce_{0.90}K_{0.10}O_2$	nd	93	5.411	3	94	84
G2–14	$Ce_{0.96}Pr_{0.02}Gd_{0.02}O_2$	nd	17	5.413	0	0	0
G2–15	$Ce_{0.94}Mn_{0.04}Sr_{0.02}O_2$	nd	13	5.409	0	0	0
G2–16	$Ce_{0.92}Ti_{0.08}O_2$	nd	16	5.408	0	0	0
G2–17	$Ce_{0.98}La_{0.02}O_2$	nd	17	5.415	0	0	0
G2–18	$Ce_{0.96}Pr_{0.02}W_{0.02}O_2$	nd	17	5.412	0	0	0
G3–01	$Ce_{0.98}K_{0.02}O_2$	nd	53	5.411	2	88	79
G3–02	$Ce_{0.98}Zr_{0.02}O_2$	nd	21	5.414	1	65	60
G3–03	$Ce_{0.98}Pr_{0.02}O_2$	nd	18	5.411	0.3	50	47
G3–04	$Ce_{0.96}Mn_{0.04}O_2$	59	13	5.408	4	85	76
G3–05	$Ce_{0.98}Al_{0.02}O_2$	nd	13	5.407	1	35	35
G3–06	$Ce_{0.93}Al_{0.02}Yb_{0.05}O_2$	nd	12	5.408	1	41	40
G3–07	$Ce_{0.96}Zr_{0.02}Cu_{0.02}O_2$	56	16	5.409	6	95	85
G3–08	$Ce_{0.96}La_{0.02}Bi_{0.02}O_2$	nd	17	5.418	9	87	84
G3–09	$Ce_{0.96}Mn_{0.02}Cu_{0.02}O_2$	nd	13	5.407	5	75	68
G3–10	$Ce_{0.96}W_{0.02}Sn_{0.02}O_2$	nd	17	5.402	6	92	82
G3–11	$Ce_{0.96}Gd_{0.05}O_2$	nd	20	5.414	1	66	61
G3–12	$Ce_{0.98}Mn_{0.02}O_2$	60	14	5.408	3	95	85
G3–13	$Ce_{0.98}Ru_{0.02}O_2$	nd	16	5.408	0	0	0
G3–14	$Ce_{0.90}Y_{0.05}Fe_{0.05}O_2$	nd	14	5.407	0	0	0

Table 1. (Continued)

Catalyst	Composition[a]	Surface area [$m^2 g^{-1}$]	Crystallite size [nm][b]	Lattice parameter [Å][c]	Activity [% H_2 converted]	H_2 oxidation selectivity [%]	Fitness value[d]
G3–15	$Ce_{0.90}Bi_{0.08}Cu_{0.02}O_2$	28	25	5.415	29[e]	83	86
G3–16	$Ce_{0.98}Pt_{0.02}O_2$	nd	16	5.411	0	0	0
G3–17	$Ce_{0.90}Cr_{0.05}Zr_{0.05}O_2$	29	22	5.405	9	95	90
G3–18	$Ce_{0.96}Sn_{0.02}Pd_{0.02}O_2$	nd	16	5.411	0	0	0

[a] Note that in the GA, concentrations of 2, 5, 8, and 10 mol% are used.
[b] Ceria has an average crystallite size of 25 nm (standard deviation = 4, $n = 4$). Doping with potassium yields larger crystallites (93 nm for **G2–13**, $Ce_{0.90}K_{0.10}O_2$, and 53 nm for **G3–01**, $Ce_{0.98}K_{0.02}O_2$). In general, however, doping decreases the crystallite size. The average crystallite size of the rest of the doped catalysts is 17 nm (standard deviation = 4, $n = 45$).
[c] Ceria has an average lattice parameter of 5.4094 Å (standard deviation = 0.0008, $n = 4$). Doping with neodymium yields a larger lattice parameter (5.4300 Å for **G1–09**, $Ce_{0.90}Nd_{0.10}O_2$). There are no trends, however, upon doping, the average lattice parameter of the rest of the doped catalysts is 5.4099 nm (standard deviation = 0.0035, $n = 46$).
[d] The fitness function is defined as: $F = [\text{selectivity} + (0.2 \times \text{activity})/120] \times 100$, and ranges from 0–100.
[e] These catalysts convert 100% of the hydrogen feed at the beginning of the reductive cycle. This does not affect the total activity, however, since all of these catalysts are depleted before the end of the reduction cycle.

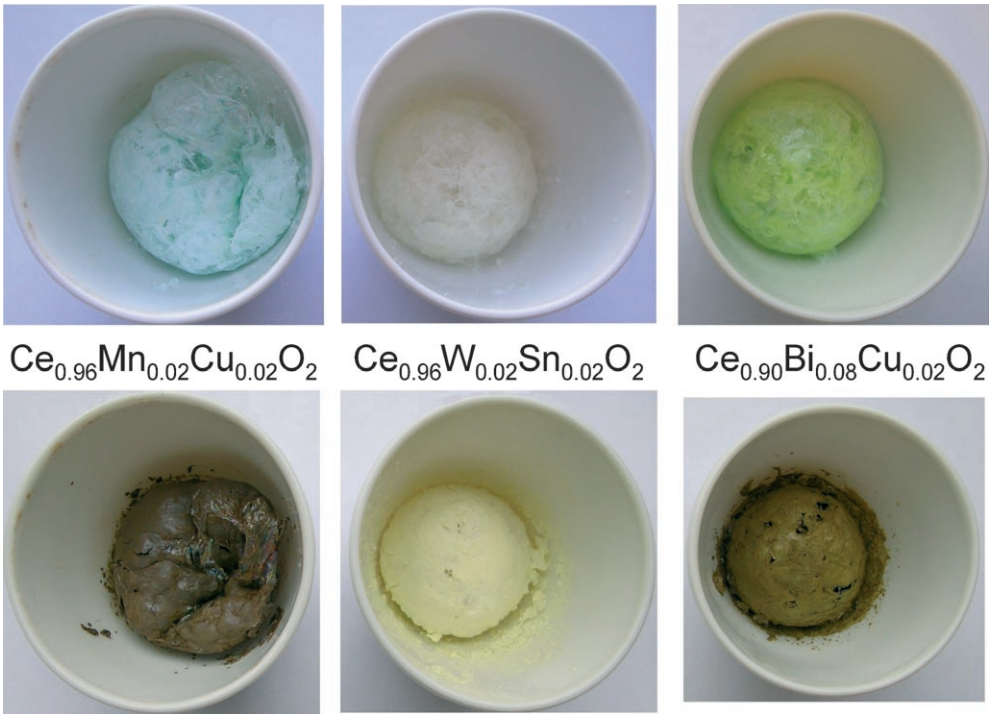

Figure 1. Photos of three catalysts (**G3–09** $Ce_{0.96}Mn_{0.02}Cu_{0.02}O_2$, **G3–10** $Ce_{0.96}W_{0.02}Sn_{0.02}O_2$ and **G3–15** $Ce_{0.90}Bi_{0.08}Cu_{0.02}O_2$) after heating under reduced pressure (*top*, mixed nitrates) and calcining (*bottom*, mixed oxides).

was characterised using powder X-ray diffraction, to ensure it consists of a uniform phase. That is, only the diffraction lines of the ceria's fluorite structure are observed, and no separate oxides of the dopants are present. Importantly, the catalysts were not prepared by impregnating CeO_2 supports. The co-melting of the cerium nitrate with the nitrates of the appropriate metals yields a well mixed liquid catalyst precursor. This allows for incorporation of the dopants into the ceria fluorite structure after calcination. However, dopant-enriched surface phases can occur for these type of catalysts, and cannot be detected by XRD.[38–40] Indeed, in the case of a copper-ceria mixed oxide, Bera et al. observed both surface enrichment and bulk incorporation of the copper.[40]

Selectivity towards Hydrogen Oxidation

In a typical reaction, 250 mg of catalyst were placed on a quartz wool plug in a quartz reactor and heated to 550 °C in 1% v/v oxygen in argon. The selectivity and activity were assessed over nine redox cycles, each consisting of an 18-min oxidation step (1% v/v O_2 in Ar), a 4-min purge in pure Ar, a 10-min reduction step (4:1:1% v/v C_3H_8:C_3H_6:H_2 in Ar), and a second 3-min purge in pure Ar. The reductive gas feed simulates the effluent from industrial propane dehydrogenation.[14] The selectivity and activity are assessed during this step using the data of 15 GC measurements, spread over the 10 min interval. The selectivity is determined as the ratio $conversion_{H_2}/conversion_{total} \times 100$, and activity is determined as the percentage of hydrogen combusted. Note that the oxygen source for this combustion is the catalyst lattice oxygen, which has to be refilled once depleted, hence the redox cycling. Figure 2 shows a scheme of the proposed redox process, where the reactor contains both the SOR (black) and dehydrogenation catalyst (grey).[41] The alkane is fed over the reactor bed and is dehydrogenated by the dehydrogenation catalyst. The formed H_2 is selectively burned from the gas mixture by the SOR (Figure 2, **A**). Since the colour of ceria changes from yellow to black when reduced, one can actually see the process. This is shown in the top picture, which is taken in our reaction set-up, after opening the reactor (catalyst used: $Ce_{0.90}Zr_{0.10}O_2$, **G1–25**). Note that in our screening reaction, the reactor only contains the SOR catalyst, over which a mixture of 4/1/1% v/v propane/propene/hydrogen is fed. The pictures were taken with a two-second time interval during the reduction step (**A**). The quick colour change is mainly caused by coking (the initial selectivity of all catalysts is low, probably due to the presence of highly reactive adsorbed oxygen). After this initial quick colour change, the bed gets darker and darker during the remainder of the reduction cycle, due to reduction of the ceria. Just before the entire SOR is spent, the bed is flushed with nitrogen to remove the reductive gases (Figure 2, **B**). Then, oxygen is fed to the reactor, reoxidising the SOR and burning-off coke from the dehydrogenation catalysts (**C**). The bottom pictures, taken at ten-second intervals, show this step for catalyst **G1–25**. When the bed is reoxidised, the oxidative gas mix is flushed out and ready for another redox cycle (Figure 2, **D**).

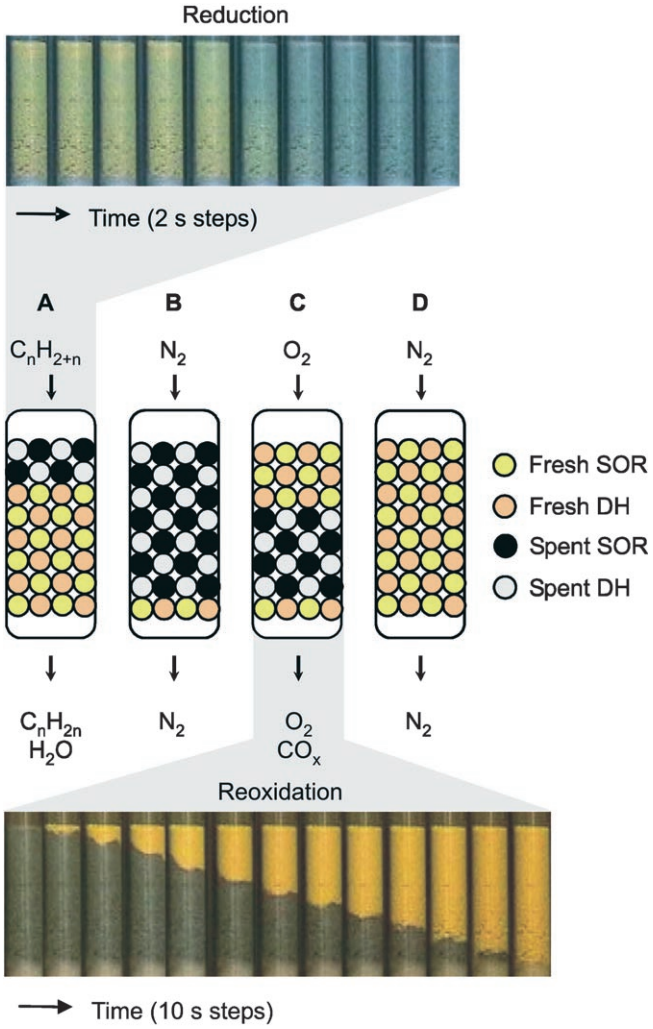

Figure 2. *Top:* pictures showing the colour change of the SOR catalyst $Ce_{0.90}Zr_{0.10}O_2$, **G1–25**, during reduction, taken at two-second time intervals. *Middle:* scheme of the proposed industrial redox dehydrogenation process. After the dehydrogenation step **A**, the bed is flushed with nitrogen (**B**), and the catalysts are regenerated through reoxidation (**C**). This burns coke from the dehydrogenation catalyst and restores the lattice oxygen of the SOR catalyst. After another nitrogen flush (**D**) the reactor is ready for the next redox cycle. *Bottom:* pictures showing the colour changes of the SOR **G1–25** during reoxidation, taken at ten-second time intervals. The difference in colour between the reduced catalyst in the top and the bottom rows of pictures is due to the different time scales (the top pictures show only the initial 12 seconds of the reduction).

Reproducibility

Table 2 shows characterisation and catalytic data of three Mn-doped catalysts, with undoped ceria added as a reference. The crystallite size of the Mn-doped catalysts is smaller than that of the undoped ceria, resulting in a larger surface area. This decrease in crystallite size occurs for most dopant types. Exceptions are Ca, W and Cr, which show comparable crystallite sizes, and K, which markedly increases the crystallite size of the ceria (the crystallite size of **G2–13**, $Ce_{0.90}K_{0.10}O_2$, is 93 nm).

The three Mn-doped catalysts show comparable selectivity, fitness, lattice parameters and surface areas.

Table 2. Catalytic and characterisation data for the magnesium-ceria mixed oxides.

Catalyst	Composition	Surface area [$m^2 g^{-1}$]	Crystallite size [nm]	Lattice parameter [Å]	Activity [% H_2 conv.]	H_2 oxidation selectivity [%]	Fitness value
G1–24	CeO_2	36[a]	25[a]	5.409[a]	0	0	0
G3–12	$Ce_{0.98}Mn_{0.02}O_2$	60	14	5.408	3	95	85
G3–04	$Ce_{0.96}Mn_{0.04}O_2$	59	13	5.408	4	85	76
G1–20	$Ce_{0.91}Mn_{0.09}O_2$	56	11	5.407	5	93	83

[a] Average of 4 samples.

The catalyst with the highest level of Mn-doping (**G1–20**), does show the highest activity.

Setting Up and Running the Algorithm

The dopants metals (M^1 and M^2 in $Ce_{1-x-y}M^1_xM^2_yO_2$) are chosen from 26 candidates, marked green in Figure 3. These were selected to cover a wide range of the periodic table. Elements that are non-solids, toxic, or are only artificially prepared were excluded (red squares in Figure 3). The white squares denote elements that are possible dopants, but not included in this study. Using these 26 dopant candidates in five concentrations (0, 2, 5, 8 and 10 mol%), and with a maximum of two dopants per catalyst, already yields a huge catalyst space – over 17000 combinations. Synthesising and testing all of these is not an option, and we therefore used a genetic algorithm to explore this catalyst space. This method is based on operators inspired by evolutionary biology, such as mutation, inheritance, natural selection and recombination.[21,42] The catalysts are treated as a group of organisms, the best of which are allowed to breed (exchange their "genetic material", i.e., the dopant type and the dopant concentration), producing a new generation (a new set of catalysts). The algorithm follows an iterative process, wherein several generations of catalysts are synthesised and tested. In each iteration, the fitness value F of each catalyst is calculated from its activity and selectivity, and used for selecting the catalysts for the next generation.

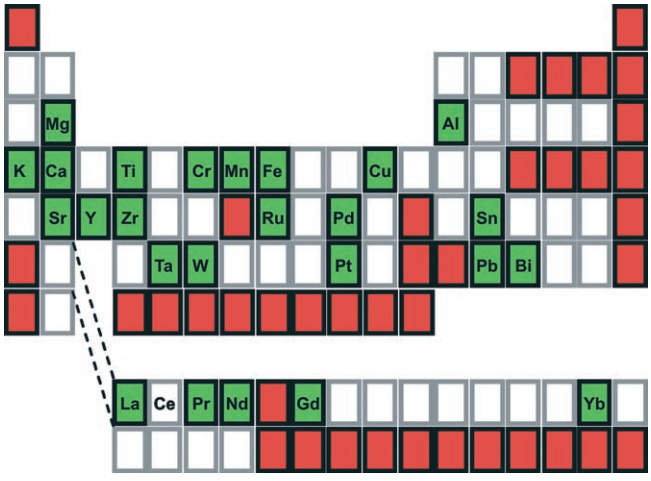

Figure 3. The periodic table showing the 26 dopant metals used in this research (green). Elements which are non-solids, toxic, or are artificially prepared were not considered as candidate and coloured red. Dopant candidates not used as yet are coloured white.

The algorithm we use does not support multi-objective optimisation (optimising several parameters at once). Therefore, the fitness value must be a single parameter, representing both the activity and selectivity of the catalysts. As noted above, the fitness function is defined as: $F = [\text{selectivity} + (0.2 \times \text{activity})/120] \times 100$, and ranges from 0–100. We decided to give more weight to the selectivity, since once a selective catalyst is discovered, its activity may still be improved, for example, by increasing its surface area. Moreover, the catalyst may be applied in other processes where the intrinsic activity is not relevant, such as co-fed oxidative dehydrogenation, where a small amount of gaseous oxygen is added to the feed,[13,14] or by applying the catalysts on an oxygen-permeable membrane, which continuously restores the lattice oxygen.[43]

The left-hand side of Scheme 2 shows a classic flow chart of a GA, the right-hand side shows the algorithm that includes a data analysis step (meta-modelling algorithm). The dashed boxes pertain to experimental steps, the rest is performed *in silico*.

Our first generation consists of 18 randomly generated catalyst formulations plus seven catalysts from a kinetic study.[11,37] The formulations are synthesised and tested, and the fitness value is calculated from the obtained activity and selectivity values. From these data, a set of new catalyst formulations ("virtual catalysts"), is generated, using three steps: selection (based on the fitness value), cross-over (the exchange of genes) and mutation (a random alteration of a small amount of genes). We use the classic GA settings of tournament selection, 50% exchange cross-over and 10% mutation. In a classic GA, n virtual catalysts are generated, where n is the size of the next generation of "real catalysts" that will be synthesised and tested (Scheme 2, left). In the "meta-modelling" algorithm we apply (Scheme 2, right), $n \times 10$ virtual

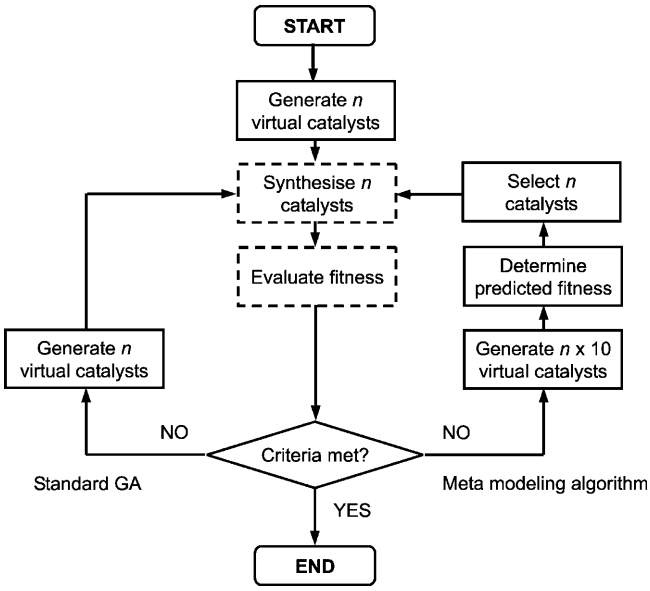

Scheme 2. General flow-chart for performing an optimisation using a genetic algorithm, with and without a data analysis step (meta-modelling algorithm). Dashed boxes denote experimental steps.

catalysts are generated. The predicted fitness of these virtual catalysts is calculated, and based on this, eighteen of the virtual catalysts are selected for synthesis and testing (real catalysts, **G2**). This pre-screening can decrease the time needed for finding the optimal catalyst.

The predicted fitness value is obtained by analysing the experimental data of the first generation of real catalysts. A simple regression is performed between the fitness and certain physical properties (descriptors) of the catalysts which may attribute to the selectivity and activity. We chose the electronegativity, ionic radius and concentration of the dopant as descriptors (*vide infra*). The program then calculates the predicted fitness value for the 250 virtual catalysts, using the regression data of the real catalysts and the descriptors of the virtual ones. For example, if there is a positive correlation between fitness value and the concentration of dopant, the virtual catalysts with high dopant concentration will get a high predicted fitness value. Finally, eighteen virtual catalysts are selected, based on their predicted fitness value, for synthesis and testing (**G2**). This meta-modelling combines the advantages of a genetic algorithm (efficient mapping of the catalyst space), and data mining (rough pre-screening of the catalysts candidates).[44–47] For **G3**, the genetic algorithm uses the fitness data of **G1** *and* **G2** (43 real catalysts) to create 430 virtual catalysts. Again, the predicted fitness value of the virtual catalysts is determined, and 18 virtual catalysts are selected for synthesis based on this predicted fitness value.

Choosing the Catalyst Descriptors

Since our reaction involves oxidation using lattice oxygen, we chose as descriptors the dopant electronegativity (influencing the strength and polarity of the metal-oxygen bond),[1,48,49] their ionic radius (which can affect the oxygen bond strength and oxygen flux by influencing the amount of stress in the ceria lattice),[50,51] the dopant concentration, and combinations of these three. A full list of the descriptors is given in the Experimental Section. Note that no experimental catalytic data were available at the start of the algorithm.

The data show little or no correlation between the fitness value and descriptors containing concentration or ionic radius. Note that the initial amount of data is low (25 catalysts after **G1**, 43 after **G2** and **G3**). Furthermore, most catalysts contain two dopants. A positive effect on the fitness value of dopant 1 may be clouded by the presence of an unselective dopant 2. Because of this, we analysed separately a set of single-dopant catalysts. This set also does not show a correlation between fitness value and either ionic (or atomic) radius, or dopant concentration. Clearly, the type of dopant has more effect on the fitness value than its concentration, and the ionic radius and fitness are unrelated.

There is a correlation between catalyst fitness value and dopant electronegativity ($R^2=0.2$, after analysis of the 43 catalysts of **G1** and **G2**). Indeed, a plot of the fitness value of the singly doped catalysts against the electronegativity of the dopants shows that most catalysts with high fitness values contain dopants with electronegativities ranging from 1.5 to 1.9 (Figure 4). The correlation is not perfect: there are also bad catalysts in this electronegativity range, and good catalysts with lower or higher electronegativities.

The algorithm uses the regression data between the descriptors and the fitness of the real catalysts to calculate the predicted fitness of the virtual catalyst set.

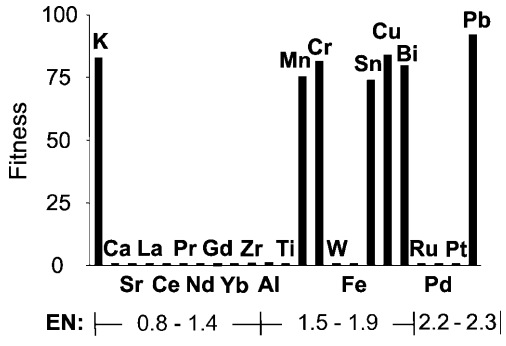

Figure 4. Fitness value against Pauling's electronegativity for the singly doped cerias. Note that the scale is not linearly increasing, for example, Ca, Sr, and La all have electronegativity of 1. Data for undoped ceria are added.

Clearly, the reliability of this predicted fitness is linked to the correlation coefficients of the regression. Since these are low, there is little correlation between the predicted and real fitness of the catalyst. Because of this, it is important to not simply choose the virtual catalysts with best predicted fitness, but to select catalysts over the entire predicted fitness range. This is also important for model validation. We therefore choose two-thirds of the virtual catalysts with high predicted fitness (75–100), and one third of the catalysts with lower predicted fitness (0–75), as candidates for the consecutive generation. Furthermore, we limited the amount of noble metal dopants Pd, Pt and Ru to a maximum of three per generation. Because of their high electronegativity, noble metals have a high predicted fitness value, but they generally result in very unselective catalysts, with high levels of coking of the hydrocarbons.

Catalyst Fitness Value Evolution over Three Generations

Figure 5 shows the average fitness value (black bars) and the percentage of catalyst with zero fitness value (hatched bars) of generations **G1**–**G3**. The data show that the average fitness value increases, and that the amount of bad catalysts decreases per generation.

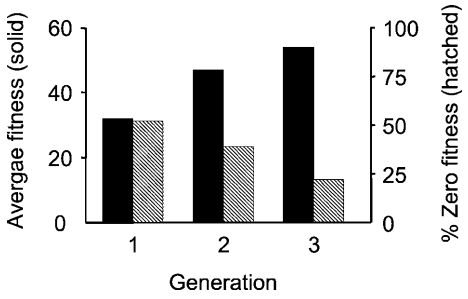

Figure 5. The average fitness (black) and the percentage of catalysts with zero fitness value (hatched) of **G1**–**G3**.

Figure 6 shows the fitness value of the individual catalysts of **G1**–**G3**, ordered by increasing fitness. In accordance with the average values shown in Figure 5, the number of catalysts with $F > 0$ increases per generation.

The data set, however, contains catalysts with a very low activity (hydrogen combustion $<2\%$). Including these catalysts allows for the discovery of a set of selective catalysts, for which the activity may still be increased, or which may be used in processes where the intrinsic activity is not relevant. For the redox process, however, the intrinsic activity is of importance, and the low activity of these catalysts renders them unsuitable. These catalysts typically have

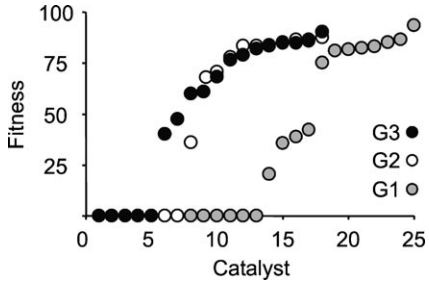

Figure 6. The fitness values of generations 1 (grey), 2 (white) and three (black) ordered for increasing fitness value. Note that there is no substantial improvement in the top catalysts between generations.

an "average" fitness value, ranging from 25 to 60, and when their fitness value is set to zero ("inactive"), the catalysts set consist of two distinct groups, one with fitness zero, the second with the fitness values ranging from 75 to 95. This clustering of the catalysts is also seen in Figure 7, where the selectivity is plotted

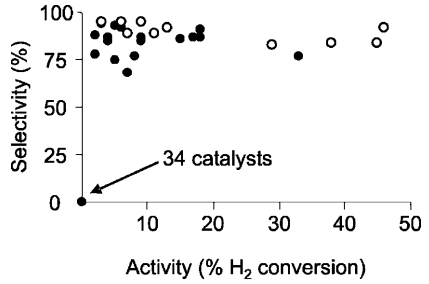

Figure 7. Selectivity versus activity for all 61 catalysts. Thirty-four of the catalysts have zero values for both selectivity and activity. The ten best catalysts, based on fitness, shown in Table 3 are marked white. The activity and selectivity of catalysts with very low activity have been set to zero.

against activity for all 61 catalysts (the activity and selectivity of the "low active" catalysts are set to zero). This figure shows that the selectivity of the catalysts is either "low" or "high," similar to the fitness values. There are no catalysts with an "average" selectivity. This is because the unselective catalysts tend to have a high activity for hydrocarbon conversion. The degree of coking, combustion or fragmentation of the hydrocarbons does vary, but these catalysts all *produce* hydrogen through hydrocarbon coking. This lack of net hydrogen combustion results in zero activity (which is defined as the percentage of hydrogen converted) and zero selectivity (the ratio of hydrogen combustion over total combustion). Therefore, these catalysts all have a fitness value of zero. The selectivity and activity of the inactive catalysts is zero as well, and they are grouped together with the unselective catalysts at the ordinate of Figure 7. The second

group of catalysts show selectivities ranging from about 70% to 95%. Note that this is still a significant difference, since high selectivities are required in the presence of the valuable hydrocarbons.

Figure 6 shows that there is a plateau in the fitness values of the best catalysts of **G1**, **G2** and **G3**. The new combinations of "good" elements of **G2** and **G3** do not lead to catalysts with a fitness value above this plateau, that is, there is little synergy between the dopants (*vide infra*). Secondly, the spread in selectivity of the "good" catalysts is much smaller than the spread in activity (Figure 7). Since the weight of the selectivity in the fitness function is much higher than that of the activity, this also contributes to the plateau in fitness.

Table 3 shows the ten best catalysts overall, selected on fitness value. These catalysts are marked white in Figure 7. The Pb-doped sample **G1–22** shows the best performance, combining high activity with high selectivity. However, during synthesis a separate PbO phase is easily formed. This was the case for samples of $Ce_{0.90}Ca_{0.05}Pb_{0.05}O_2$, $Ce_{0.87}Pb_{0.05}Sr_{0.08}O_2$, and $Ce_{0.93}Pb_{0.05}Zr_{0.02}O_2$.[52] Even monodoped Pb-Ce samples are difficult to prepare without formation of PbO. Because of this, no lead-containing samples are present in **G2** and **G3**. It is interesting to note that the selectivity of the catalysts containing a separate PbO phase is as high as for the Pb-doped ceria. However, previous studies with alumina- and silica-supported lead oxides have shown that these catalysts are not stable under the high temperature redox cycling.[17]

High selectivities are obtained also with the Cr/Zr-doped and Zr/Cu-doped catalysts (**G3–17** and **G2–06**, respectively), albeit at lower activity. The next best catalysts all contain Bi, and show high activities. Indeed, analysis of the five most active catalysts shows that these contain either lead (**G1–22**) or bismuth (**G2–07**, **G2–03**, **G1–19**, and **G3–15**). All mixed oxides of the set, with a Bi concentration of 5 mol% or higher, are amongst the most active catalysts. However, adding Bi results in some combustion of the propene feed, giving lower selectivities ($<85\%$).

The most active catalysts are so active that they combust *all* of the hydrogen during part of the reductive cycle (100% conversion). It is known that the presence of hydrogen can limit hydrocarbon combustion. Indeed, increasing the amount of hydrogen for **G1–19**, $Ce_{0.90}Bi_{0.10}O_2$, decreases the amount of propene combustion, and so increases the selectivity. This strategy is not practical, however, for the oxidative dehydrogenation process, since adding hydrogen shifts the equilibrium away from the desired products. Interestingly, the Pb-doped ceria **G1–22** combusts all of the hydrogen as well, but without burning any of the hydrocarbons. Apparently, the lead has an intrinsically lower affinity for converting propene as compared to bismuth, under these reaction conditions.

Parameters Influencing Activity and Selectivity

Table 3 shows that generally, the ten best catalysts have a somewhat lower crystallite size as compared to undoped ceria, their surface area is higher (these two are correlated), and their lattice parameters are about the same. This, however, is also the case for most low fitness value catalysts (see also Table 1). For example, **G1–23**, $Ce_{0.90}Pd_{0.10}O_2$, has a small crystallite size (13 nm), a high surface area ($72\ m^2\ g^{-1}$) and a lattice

Table 3. Catalysts with the highest fitness.

Catalyst	Composition[a]	Surface area [$m^2\ g^{-1}$]	Crystallite size [nm]	Lattice parameter [Å]	Activity [% H_2 conversion]	H_2 oxidation selectivity [%]	Fitness value
G1–22	$Ce_{0.92}Pb_{0.08}O_2$	56	13	5.411	46[b]	92	93
G3–17	$Ce_{0.90}Cr_{0.05}Zr_{0.05}O_2$	29	22	5.405	9	95	90
G2–06	$Ce_{0.84}Zr_{0.08}Cu_{0.08}O_2$	54	17	5.411	13	92	88
G2–07	$Ce_{0.87}Bi_{0.08}Sn_{0.05}O_2$	55	14	5.411	45[b]	84	87
G2–03	$Ce_{0.90}Cr_{0.05}Bi_{0.05}O_2$	31	28	5.412	38[b]	84	87
G3–15	$Ce_{0.90}Bi_{0.08}Cu_{0.02}O_2$	28	25	5.415	29[b]	83	86
G3–12	$Ce_{0.98}Mn_{0.02}O_2$	60	14	5.408	3	95	85
G3–07	$Ce_{0.96}Zr_{0.02}Cu_{0.02}O_2$	56	16	5.409	6	95	85
G2–12	$Ce_{0.90}Al_{0.02}Cu_{0.05}O_2$	52	14	5.409	11	89	85
G1–18	$Ce_{0.90}Cu_{0.10}O_2$	47	15	5.411	7	89	85
G1–24	CeO_2[c]	36[d]	25[d]	5.409[d]	0	0	0

[a] Note that in the GA, concentrations of 2, 5, 8, and 10 mol% are used.
[b] These catalysts convert 100% of the hydrogen feed at the beginning of the reductive cycle. This does not affect the total activity, however, since all of these catalysts are depleted before the end of the reduction cycle.
[c] Added for reference.
[d] The values are the average of 4 samples.

parameter of 5.411. Still, this catalyst shows a high degree of hydrocarbon combustion and coking. This shows that the dopant type is more important for selectivity than general properties such as the crystallite size or lattice parameter. Concerning activity, studies of undoped ceria showed that a smaller crystallite size and larger surface area increases the amount of oxygen released below 600 °C.[53,54] For the activity in the selective hydrogen combustion, however, the type of dopant added has a larger effect. For example, the crystallite size of the Cr/Bi-doped ceria **G2–03** is larger than that of the Zr/Cu-doped ceria **G2–06**, and its surface area is smaller. Still, **G2–03** is three times as active as **G2–06**.

The activity of copper-containing catalysts is increased by the addition of certain dopants. The monodoped Cu-Ce catalysts only show average activities: **G1–18**, containing 10 mol% Cu, combusts 7% of the hydrogen feed, samples containing 7 mol% and 3 mol% of Cu show comparable values (see Table 1). However, addition of calcium (**G2–02**) or magnesium (**G2–04**) increases this activity to 18% and 17%, respectively. The addition of calcium also increases the time in which the catalyst is active. This prevents the typical coking of the hydrocarbons, which is normally seen for Cu-Ce catalysts after their oxygen has been depleted.

Catalyst Stability

Catalyst **G3–17** ($Ce_{0.90}Cr_{0.05}Zr_{0.05}O_2$) was subjected to a total of 250 redox cycles.[55] Figure 8 shows that there is some variation in activity, but selectivity is uncompromised. Furthermore, XRD analysis of the spent catalyst shows no phase segregation, and no noteworthy increase in crystallite size (i.e., no sintering).

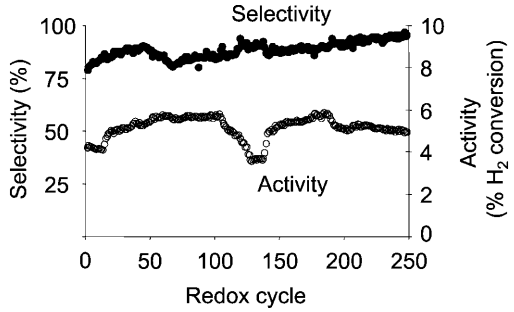

Figure 8. Selectivity (●) and activity (○) for **G3–17** ($Ce_{0.90}Cr_{0.05}Zr_{0.05}O_2$) for a total of 250 redox cycles (148 h on stream). Measurements were performed in two batches of 125 cycles, the catalyst was stored under air at room temperature in between the batches. Note that the activity (% hydrogen conversion) is lower than that presented in Table 1 and Table 3, since fewer GC measurements were taken each cycle.

The Relationship between Dopant Type and Fitness

Table 3 shows that the best catalysts contain Pb, Cr, Bi, Zr and Cu. These catalysts, however, often contain two dopants. Analysis of monodoped catalysts shows that indeed most of the aforementioned metals yield catalysts with a high fitness (Figure 4). Generally, the type of dopant added results in catalysts with three types of behaviour: "good," "bad," and "inactive" (Figure 9). "Bad" dopants, such as Pd, Ru, and Fe, result in unselective catalysts, which coke and combust part of the hydrocarbon feed, and therefore have fitness zero. "Inactive" dopants, such as Ca, Ti or Pr, yield inactive catalysts which are also given a fitness of zero. "Good" dopants, such as Pb, Cu, Bi, yield catalysts with a relatively high selectivity and activity, with fitness ranging from 75–95. For example, the eight catalysts of the set containing copper, either mono- or bidoped, have an average fitness of 83, with a standard deviation of 6. The seven bismuth-containing catalysts have an average fitness of 83, with a standard deviation of 7.

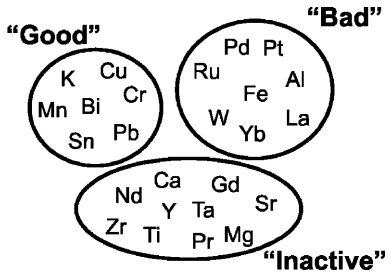

Figure 9. The dopants classified according to their catalytic behaviour, based on the performance of single-dopant catalysts. Some distinction can be made for the bad metals: addition of Fe, Pd, Ru, and Pt results in very high amounts of coking and combustion of the hydrocarbons, where this is much lower for the metals W, Yb and La. Also, when La, W and Al are added at low concentration (2 mol%), the distinction between "bad" and "inactive" becomes less clear. The metals Sm, Ta, and Mg have has not been tested as single dopant. The behaviour of Ta and Mg is derived from its combination with an inactive metal.

The behaviour of catalysts containing two dopants can be predicted from that of the monodoped ones, as shown in Table 4. For example, combining a bad dopant with a "good," "inactive," or "bad" one, yields a "bad" catalyst. This is because the "bad" dopant still results in coking of the hydrocarbons, yielding a low selectivity. The combination of a "good" and "inactive" dopant yields a "good" catalyst, and so does the combination of two "good" dopants. That is, there is not much synergy, and because of this, a plateau is present around fitness 80 (Figure 6). This is also caused by the high weight of selectivity in the fitness function (comprising 80% of the fitness value). The

Table 4. Rules for the performance of catalysts containing combinations of "good," "bad" and "inactive" metals.

Number	Combination of dopant type	Catalyst performance	Typical fitness value
1	"good"	"good"	75–95
2	"good" + "inactive"	"good"	75–95
3	"good" + "good"	"good"	75–95
4	"inactive"	"bad"	0
5	"inactive" + "inactive"	"bad"	0
6	"bad" + "inactive"	"bad"	0
7	"bad" + "good"	"bad"	0
8	"bad" + "bad"	"bad"	0
9	"bad"	"bad"	0

combination of two "good" (selective) dopants yields catalysts with comparable selectivity to that of the separate dopants, resulting in the plateau in fitness value.

Almost all catalyst with two dopants comply with the rules given in Table 4. The only exceptions are the increase in activity of certain copper-containing catalysts (*vide supra*), and catalysts containing iron. The fitness of iron-doped ceria itself is low (**G1–17**, $Ce_{0.90}Fe_{0.10}O_2$), but the addition of some Cr yields a highly selective catalyst (**G1–03** $Ce_{0.89}Cr_{0.02}Fe_{0.09}O_2$). Addition of 2 mol% Mn and Zr is beneficial as well, albeit to a lesser extent, addition of Y has no effect on catalyst performance (catalysts **G2–05**, **G2–10**, and **G3–14**, respectively).

Conclusions

We have successfully applied a genetic algorithm for screening doped ceria catalysts for the selective combustion of hydrogen from a mixture with propane and propene. Three generations, with a total of 61 doped ceria catalysts, have been synthesised and tested. Each generation shows a higher average fitness value and lower amount of catalysts with a fitness value of zero. The dopant type has a large effect on both the activity and selectivity of the catalyst. Three types of catalytic behaviour are identified, depending on the dopant added: the catalysts are either selective, inactive or unselective. The best results are obtained when doping with lead, chromium, copper, manganese and tin ("good" dopants). Interestingly, most of these metals have electronegativities ranging from 1.5–1.9.

Generally, the properties of catalysts containing two dopants can be predicted from the behaviour of singly doped ones. Incorporation of a "bad" dopant yields an unselective catalysts, regardless of the second dopant added, and the combination of two "good" dopants yields a catalyst with a fitness comparable to catalysts doped with a single "good" dopant. Synergy does occur for certain copper- and iron-containing catalysts. The activity of copper-doped catalysts doubles when adding calcium or magnesium, and the selectivity of iron-doped catalysts is improved by adding chromium, manganese or zirconium. The stability under the high temperature redox cycling is excellent. A Cr- and Zr-doped catalyst was selective and active over 250 redox cycles (a total of 148 h on stream), with no phase segregation or increase in particle size.

Experimental Section

Materials and Instrumentation

Chemicals were purchased from Sigma–Aldrich, Merck, The British Drug Houses Ltd. or Koch-Light Laboratories Ltd and used as received. Gases had a purity of 99.5% or higher and were purchased from Praxair. The O_2, He, Ar and N_2 streams were purified further over mol sieves and/or BTS columns. All gas flows were controlled by Bronkhorst mass flow controllers. The specific surface areas were measured by N_2 adsorption at 77 K on a Sorptomatic 99 (CE Instruments) and evaluated using the BET equation. Powder X-ray diffraction measurements were performed using a Philips PW-series X-ray diffractometer with a Cu tube radiation source ($\lambda = 1.54$ Å), a vertical axis goniometer and a proportional detector. The 2θ detection measurement range was 10°–93° with a 0.02° step size and a five-second dwell time. Lattice constants and crystallite sizes were obtained after Rietveld refinement (structure fit) using PANalytical's X′pert software package. Inductive coupled plasma (ICP) measurements were performed on a Perkin Optima 3000XL ICP instrument. ICP samples were prepared using a Perkin–Elmer Micro Wave Sample Preparation System. The software used is OptiCat,[56] allowing for designing and exploiting evolutionary algorithms, and Statistica V6.1 for the data mining.[57]

Procedure for Catalyst Synthesis

Some adjustments were made to the synthesis procedure described previously.[11] The metal nitrate precursors (or chlorides or ammonium metallates, where nitrates were not available) were weighed into a crucible and placed on a heater. When liquefied, they were mixed with a spatula. If necessary, 2–6 drops of water were added to aid the solution of the precursors. After about 5 min, the crucible was placed in a 140 °C vacuum oven. Pressure was reduced to <10 mbar in about 10 min. The latter was performed carefully to prevent vigorous boiling. After 4 h, the crucible was placed in a muffle oven and calcined for 5 h at 700 °C in static air (ramp rate: 300 °C/h). The resulting solid was pulverised, ground and sieved in fractions of 125–212 μm (selectivity assessment) and <125 μm (XRD and BET measurements). The final metal concentration was calculated from the amount of precursor weighed in, corrected for the water content as determined on catalysts **G1–01** to **G1–18** by ICP.[11]

Procedure for Selective Hydrogen Combustion Experiments

Activity and selectivity were determined on a fully automated system built in-house, which was described in detail previously.[11] In a typical experiment, about 250 mg of sample (125–212 μm) were placed on a quartz wool plug in a 4-mm i.d. quartz reactor. The reactor was placed in a water-cooled oven and heated to 550 °C at 1200 °C/h, under oxygen flow. At this temperature, redox cycling was started. The selectivity was determined by GC during the 10 min reduction in 4:1:1% v/v C_3H_8:C_3H_6:H_2 in Ar. The 4:1:1 ratio of reductive gases is chosen since this is the equilibrium mixture of a conventional dehydrogenation catalyst.[14] After a 4-min purge step (pure Ar), the sample was reoxidised for 18 min in 1% v/v O_2 in Ar. The redox cycle is completed by another purge step in pure Ar. The total flow rate was kept at 50 mL min^{-1} in each step. The selectivity is determined as the ratio H_2 conversion:total conversion. Activity is determined as the percentage hydrogen combusted during the reduction step. Both selectivity and activity are averaged over eight redox cycles

Procedure for ICP Analysis

ICP was performed on catalysts **G1–01** to **G1–18**, containing all dopant types used in this study. The metals were brought in solution by heating approximately 50 mg samples in 6 mL *aqua regia* to 170–200 °C using a microwave oven. These temperatures were held for 25 min, during which the pressure typically rose to 40–55 bar. After cooling, the volume was brought to 100 mL with demineralised water. Before analysis this sample was diluted 100 times. Cerium recovery from a pure ceria sample using this method was 98.3% (average of 6 measurements). W, K, and Ta could not be determined using this method, probably due to limited solubility of the oxides. An alternative method involving gentle heating in a mixture of 5 mL concentrated HF and 2 mL 2 M H_2SO_4 for 2 h did not work either. Therefore, the concentration of these elements was calculated from the amount of precursors weighed.

GA Programming, Descriptors and Implementation

The GA part uses binary encoding of the variables; the dopants are encoded on 9 bits, while their quantity is coded on 6 bits. The statistical model used for the meta-modelling is a classic linear regression. The descriptors are the total dopant concentration (mol%), the ionic radius of dopant 1, the ionic radius of dopant 2, the electronegativity of dopant 1 (Pauling's scale), the electronegativity of dopant 2, the concentration × ionic radius of dopant 1, the concentration × ionic radius of dopant 2, the concentration × electronegativity of dopant 1, and the concentration × electronegativity of dopant 2.

Acknowledgements

We thank Dr. M. C. Mittelmeijer-Hazeleger the BET surface area measurements, A. C. Moleman and W. F. Moolhuijzen for help with the XRD measurements, A. J. van Wijk and L. Hoitinga for performing the ICP measurements, and NWO–ASPECT for financial support and feedback.

References

[1] R. K. Grasselli, *Top. Catal.* **2002**, *21*, 79.
[2] N. Alperowicz, *Chem. Week* **2006**, *168*, 17.
[3] G. Parkinson, *Chem. Eng. Prog.* **2004**, *100*, 8.
[4] J. Plotkin, E. Glatzer, *Eur. Chem. News* **2005**, *82*, 20.
[5] A. Scott, M. Bryner, *Chem. Week* **2007**, *169*, 14.
[6] F. Cavani, N. Ballarini, A. Cericola, *Catal. Today* **2007**, *127*, 113.
[7] R. Grabowski, *Catal. Rev. – Sci. Eng.* **2006**, *48*, 199.
[8] L. Låte, J. I. Rundereim, E. A. Blekkan, *Appl. Catal. A: Gen.* **2004**, *262*, 53.
[9] L. Låte, W. Thelin, E. A. Blekkan, *Appl. Catal. A: Gen.* **2004**, *262*, 63.
[10] G. Rothenberg, E. A. de Graaf, A. Bliek, *Angew. Chem. Int. Ed.* **2003**, *42*, 3366.
[11] J. H. Blank, J. Beckers, P. F. Collignon, F. Clerc, G. Rothenberg, *Chem. Eur. J.* **2007**, *13*, 5121.
[12] E. A. de Graaf, G. Rothenberg, P. J. Kooyman, A. Andreini, A. Bliek, *Appl. Catal. A: Gen.* **2005**, *278*, 187.
[13] R. K. Grasselli, D. L. Stern, J. G. Tsikoyiannis, *Appl. Catal. A: Gen.* **1999**, *189*, 9.
[14] R. K. Grasselli, D. L. Stern, J. G. Tsikoyiannis, *Appl. Catal. A: Gen.* **1999**, *189*, 1.
[15] J. G. Tsikoyiannis, D. L. Stern, R. K. Grasselli, *J. Catal.* **1999**, *184*, 77.
[16] C. H. Lin, K. C. Lee, B. Z. Wan, *Appl. Catal. A: Gen.* **1997**, *164*, 59.
[17] L. M. van der Zande, E. A. de Graaf, G. Rothenberg, *Adv. Synth. Catal.* **2002**, *344*, 884.
[18] A. Trovarelli, C. de Leitenburg, M. Boaro, G. Dolcetti, *Catal. Today* **1999**, *50*, 353.
[19] J. H. Holland, *Adaptation in Natural and Artificial Systems*, The University Press of Michigan, Ann Arbor, MI, **1975**.
[20] D. Farrusseng, F. Clerc, *Appl. Surf. Sci.* **2007**, *254*, 772.
[21] D. E. Goldberg, *Genetic Algorithms in Search, Optimization and Machine Learning*, Addison-Wesley, Reading, MA, **1989**.
[22] D. Wolf, O. V. Buyevskaya, M. Baerns, *Appl. Catal. A: Gen.* **2000**, *200*, 63.
[23] O. V. Buyevskaya, D. Wolf, M. Baerns, *Catal. Today* **2000**, *62*, 91.
[24] O. V. Buyevskaya, A. Brückner, E. V. Kondratenko, D. Wolf, M. Baerns, *Catal. Today* **2001**, *67*, 369.
[25] U. Rodemerck, D. Wolf, O. V. Buyevskaya, P. Claus, S. Senkan, M. Baerns, *Chem. Eng. J.* **2001**, *82*, 3.
[26] S. Moehmel, N. Steinfeldt, S. Engelschalt, M. Holena, S. Kolf, A. Baerns, U. Dingerdissen, D. Wolf, R. Weber, M. Bewersdorf, *Appl. Catal. A: Gen.* **2008**, *334*, 73.
[27] Y. Watanabe, T. Umegaki, M. Hashimoto, K. Omata, M. Yamada, *Catal. Today* **2004**, *89*, 455.
[28] K. Omata, Y. Watanabe, M. Hashimoto, T. Umegaki, M. Yamada, *Ind. Eng. Chem. Res.* **2004**, *43*, 3282.
[29] K. Omata, M. Hashimoto, Y. Watanabe, T. Umegaki, S. Wagatsuma, G. Ishiguro, M. Yamada, *Appl. Catal. A: Gen.* **2004**, *262*, 207.

[30] F. Clerc, M. Lengliz, D. Farrusseng, C. Mirodatos, S. R. M. Pereira, R. Rakotomalala, *Rev. Sci. Instrum.* **2005**, *76*, 062208.
[31] Y. Yamada, T. Kobayashi, *J. Jpn. Petrol. Inst.* **2006**, *49*, 157.
[32] G. Kirsten, W. F. Maier, *Appl. Surf. Sci.* **2004**, *223*, 87.
[33] C. Breuer, M. Lucas, F. W. Schutze, P. Claus, *Comb. Chem. High T. Scr.* **2007**, *10*, 59.
[34] O. C. Gobin, A. M. Joaristi, F. Schuth, *J. Catal.* **2007**, *252*, 205.
[35] D. K. Kim, W. F. Maier, *J. Catal.* **2006**, *238*, 142.
[36] A. Corma, J. M. Serra, A. Chica, *Catal. Today* **2003**, *81*, 495.
[37] J. H. Blank, J. Beckers, P. F. Collignon, G. Rothenberg, *ChemPhysChem.* **2007**, *8*, 2490.
[38] P. J. Scanlon, R. A. M. Bink, F. P. F. van Berkel, G. M. Christie, L. J. van IJzendoorn, H. H. Brongersma, R. G. van Welzenis, *Solid State Ionics* **1998**, *112*, 123.
[39] G. Rothenberg, E. A. de Graaf, J. Beckers, A. Bliek, *Catal. Org. React.* **2005**, *104*, 201.
[40] P. Bera, K. R. Priolkar, P. R. Sarode, M. S. Hegde, S. Emura, R. Kumashiro, N. P. Lalla, *Chem. Mater.* **2002**, *14*, 3591.
[41] E. A. de Graaf, G. Zwanenburg, G. Rothenberg, A. Bliek, *Org. Process. Res. Dev.* **2005**, *9*, 397.
[42] D. E. Sadava, *Life: The Science of Biology*, Sinauer Associates, Inc., Sunderland, MA, **2008**, p 207.
[43] J. A. Dalmon, A. Cruz-Lopez, D. Farrusseng, N. Guilhaume, E. Iojoiu, J. C. Jalibert, S. Miachon, C. Mirodatos, A. Pantazidis, M. Rebeilleau-Dassonneville, Y. Schuurman, A. C. van Veen, *Appl. Catal. A: Gen.* **2007**, *325*, 198.
[44] Y. Yin, *Soft Computing* **2003**, *9*, 3.
[45] F. Clerc, *PhD thesis*, Claude Bernard University, France, **2006**.
[46] G. Rothenberg, *Catal. Today* **2008**, *137*, 2.
[47] V. Prasad, D. G. Vlachos, *Ind. Eng. Chem. Res.* **2008**, DOI: 10.1021/ie800343s.
[48] R. T. Sanderson, *J. Am. Chem. Soc.* **1983**, *105*, 2259.
[49] R. Burch, D. J. Crittle, M. J. Hayes, *Catal. Today* **1999**, *47*, 229.
[50] M. Mogensen, N. M. Sammes, G. A. Tompsett, *Solid State Ionics* **2000**, *129*, 63.
[51] V. Butler, C. R. A. Catlow, B. E. F. Fender, J. H. Harding, *Solid State Ionics* **1983**, *8*, 109.
[52] For some of these catalysts, PbO is not detected by XRD, but the sample is inhomogeneous in colour. The PbO clusters may be below the XRD detection limit (~3 nm).
[53] E. Aneggi, M. Boaro, C. de Leitenburg, G. Dolcetti, A. Trovarelli, *J. Alloy Compd.* **2006**, *408*, 1096.
[54] F. Giordano, A. Trovarelli, C. de Leitenburg, M. Giona, *J. Catal.* **2000**, *193*, 273.
[55] Two batches of 125 cycles (73 h on stream) were performed on the same catalyst.
[56] F. Clerc, *OptiCat – A Combinatorial Optimisation Software*, OptiCat can be downloaded free of charge from http://eric.univ-lyon2.fr/~fclerc/.
[57] *Statistica 6.1* is commercially avaliable from StatSoft, Inc., 1984–2008, 2300 East 14th Street, Tulsa, OK 74104, USA.

